International Journal of Heat and Mass Transfer 52 (2009) 1677–1689

Contents lists available at ScienceDirect

International Journal of Heat and Mass Transfer

journal homepage: www.elsevier.com/locate/ijhmt

3D hybrid Cartesian/immersed-boundary finite-element analysis of heat and flow patterns in a two-roll mill

C.L. Chiu, C.M. Fan, D.L. Young *

Department of Civil Engineering & Hydrotech Research Institute, National Taiwan University, Taipei 10617, Taiwan

ARTICLE INFO

Article history:
Received 27 September 2007
Received in revised form 8 September 2008
Available online 29 November 2008

Keywords:
Three-dimensional Navier–Stokes equations
Two-roll mill
Forced convection
Hybrid Cartesian/immersed-boundary method
Finite-element method

ABSTRACT

A fully three-dimensional time-dependent Navier–Stokes model with forced convection is developed to numerically investigate the heat and flow patterns of the two-roll mill system with two inner rotating cylinders. Such direct numerical simulations are usually limited by the difficulties from huge computational cost and complex boundary treatment. For a fast numerical process, we can use the operator-splitting scheme with the BTD term to advance the solution in temporal evolution. To implement the calculation over a Cartesian grid, the hybrid Cartesian/immersed-boundary finite-element method is employed for spatial discretization. In the authors' previous study [D.L. Young, C.L. Chiu, C.M. Fan, A hybrid Cartesian/immersed-boundary finite-element method for simulating heat and flow patterns in a two-roll mill, Numer. Heat Transfer B 51 (3) (2007) 251–274], we have developed a simplified 2D numerical model to analyze the heat and flow patterns on the cross section of two-roll-mill flow under the assumption of infinite length in the third (vertical) direction. However, the 2D solutions could not completely represent the realistic physical phenomena unless a 3D algorithm is developed. In this study we then paid the particular attention to develop a 3D model to investigate the vertical heat and flow behaviors, including 3D features of the vortex structure, periodic oscillation and chaotic instabilities. It is found that the proposed 3D model is able to cover the 2D features if the assumptions of 2D conditions are fulfilled.

1. Introduction

Researchers in all aspects of theoretical, computational and experimental investigations for decades have focused on flow transition and hydrodynamic instability in rotating systems since it is an important subject in fluid mechanics. Among these investigations, the Taylor–Couette problem is the most well-known benchmark for understanding the mechanisms of flow instabilities and vertical vortical motions. The vortex structure, the hydrodynamic instability and the mass transfer of flows are of particular interest for fluid mechanists. These phenomena are usually studied by analytical or experimental methods [1,2]. Recently, with the vast improvement of computer technology, the 3D numerical Navier–Stokes models were developed to provide the detailed information of the Taylor–Couette flows. Rudman [3] examined the effect of wavy motion on mixing and particle transport in the wavy vortex regime of Taylor–Couette flow. Liao et al. [4] investigated the flow patterns for the states or regimes of steady circular Couette flow, steady Taylor vortices and the onset of periodic spiral vortices.

The flow device of a two-roll mill is another interesting alternative of rotating system, which has been widely used for studies in chaotic advection, drop and bubble dynamics [5], etc. Due to the geometric complexity, the analytical and numerical methods are usually limited to the assumptions of axisymmetry and even inertia force free to simplify the analysis. Reyes and Geffroy [6] provided a closed-form analytical solution for the Stokes flow generated by a co-rotating two-roll mill. On the other hand, Price et al. [7] in contrast applied a least-squares approach to calculate the Stokes flow in the two-roll-mill domain, and compared the numerical results with some experimental data. Hills [8] investigated the flow field for a two-roll mill using a finite-difference scheme over a special-arrangement Cartesian grid. However, it is observed that in Hills' study the variable spacing must comply satisfactorily with the circular boundaries. In fact, the capability to handle complex geometry problems remains a challenging task in the realm of computational fluid dynamics especially for 3D heat and flow patterns.

The computational fluid dynamics community recently is particularly interested in the Cartesian grid-based method, since the governing equations with complicated geometry could be discretized by a Cartesian grid that generally does not conform to the immersed boundaries. It can greatly simplify grid generation while retaining the efficiency of Cartesian solvers. A major

* Corresponding author. Tel./fax: +886 2 23626114.
E-mail address: dlyoung@ntu.edu.tw (D.L. Young).

0017-9310/$ - see front matter © 2009 Published by Elsevier Ltd.
doi:10.1016/j.ijheatmasstransfer.2008.09.019

Nomenclature

f	momentum body force
H	height of circular cylinder
h	energy body force
P	point in Cartesian coordinates
p	dimensionless pressure
R	dimensionless radius of outer cavity
r	dimensionless radius of inner cylinder
Pr	Prandtl number
Re	Reynolds number
T	dimensionless temperature
t	dimensionless time
u	dimensionless velocity vector
$\mathbf{u}^*$	intermediate velocity
u, v, w	dimensionless velocity components
x, y, z	dimensionless coordinates
∇	del operator
∇^2	Laplacian
Δt	time increment
ϕ_i	angular velocity of inner cylinder, $i = 1, 2$

Superscript and subscript

n	*nth* time step
n + 1	(*n*+1)th time step
b	desired boundary condition

challenge for these methods is to accurately represent the effect of immersed boundaries, since the immersed boundary usually does not coincide with the Cartesian grid points. Among the Cartesian grid-based methods, the hybrid Cartesian/immersed-boundary method [9–13] is especially suitable for problems with the complex geometry and prescribed moving boundary, since it does not require additional free parameters and numerical remesh procedure. In recent years many papers have focused on the improvement of interpolation schemes for imposing the boundary conditions on the Cartesian grids. Mohd-Yusof [9]

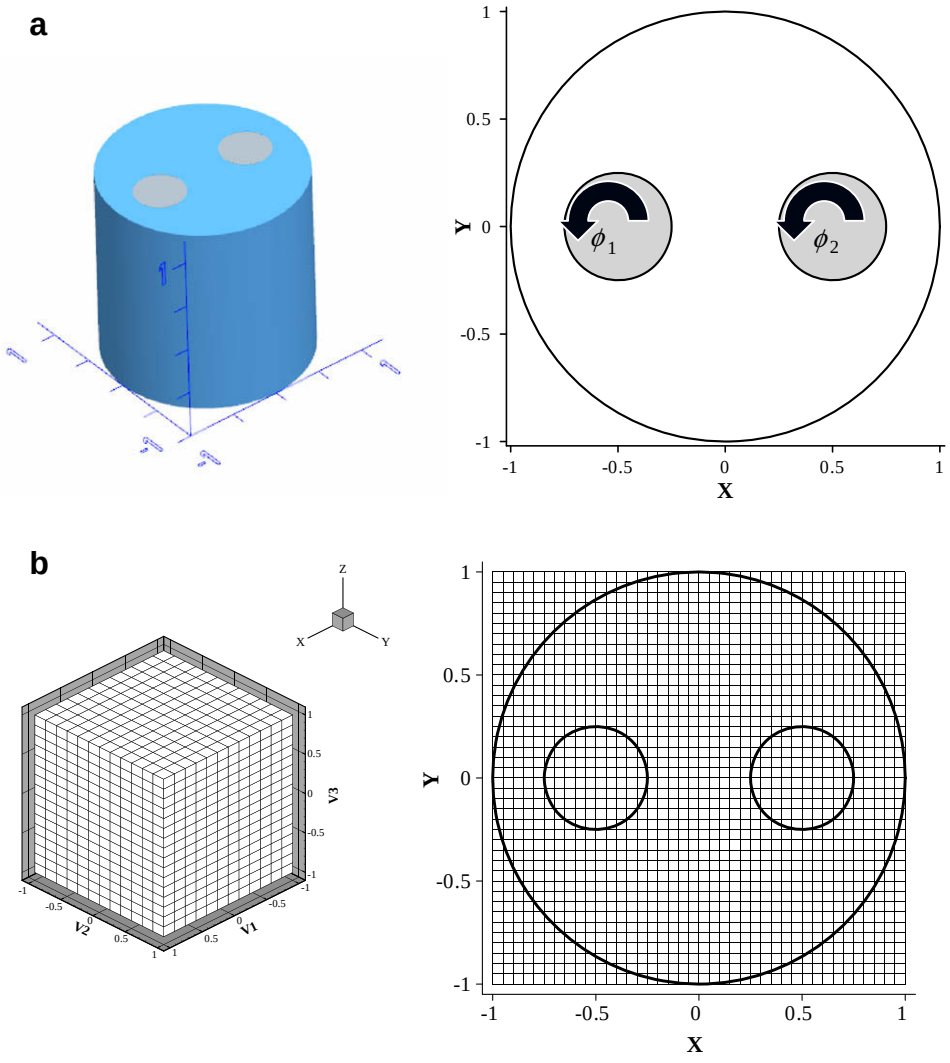

Fig. 1. (a) Computational geometry and (b) mesh layout for the two-roll-mill flow with inner rotating cylinders in view of full domain (left) and cross section (right).

applied the direct forcing concept only on the immersed boundary or inside the body, and the interpolation schemes were implemented in the B-spline direction. Besides Fadlun et al. [10] reconstructed the velocity at the first grid point external to the immersed boundary. Balaras [11] proposed a simple interpolation scheme where the interpolation direction was normal to

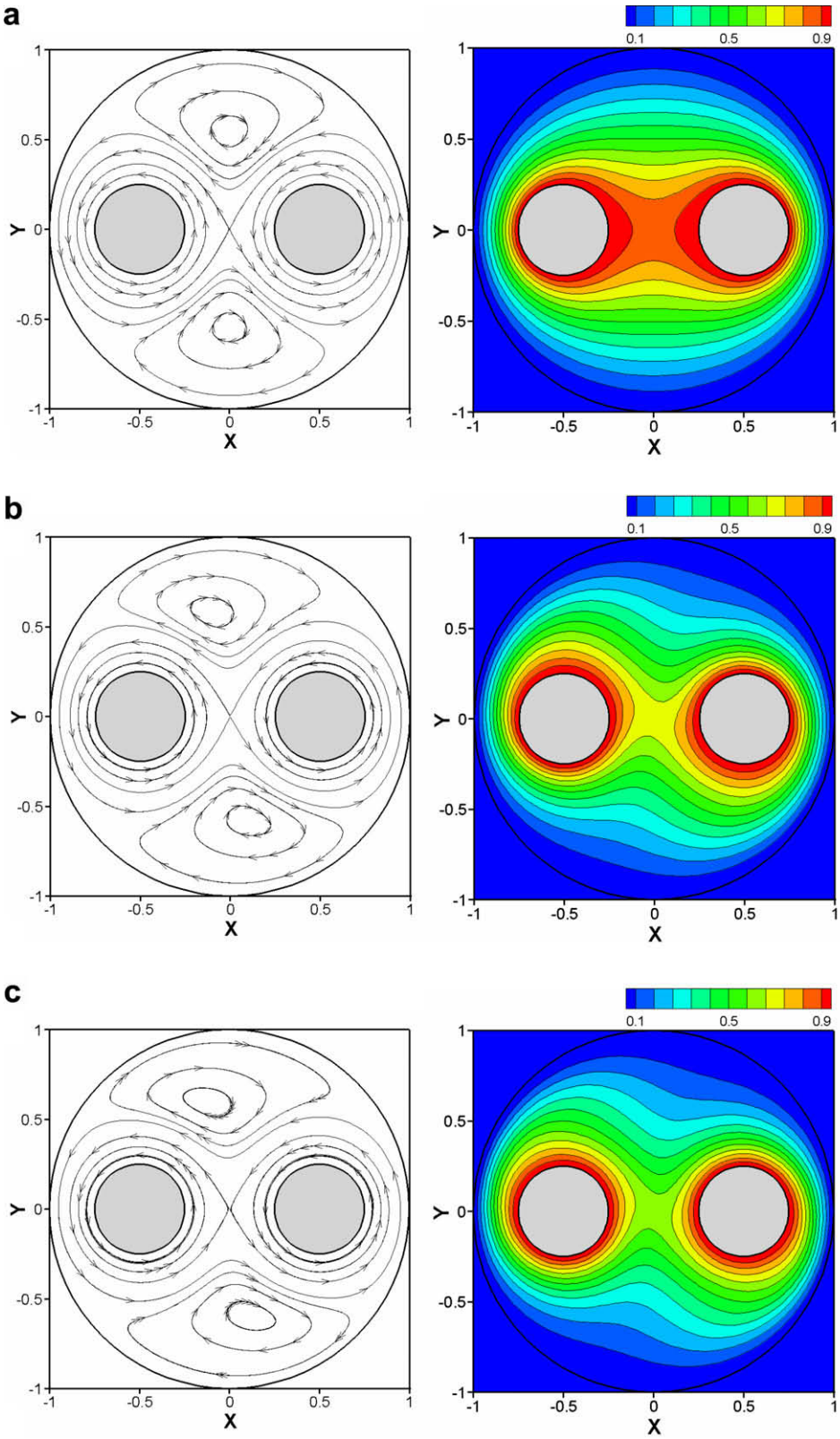

Fig. 2. Streamlines (left) and isotherms (right) of a co-rotating two-roll mill on $z = 0$ plane for: (a) Re = 0.1; (b) Re = 100; (c) Re = 200.

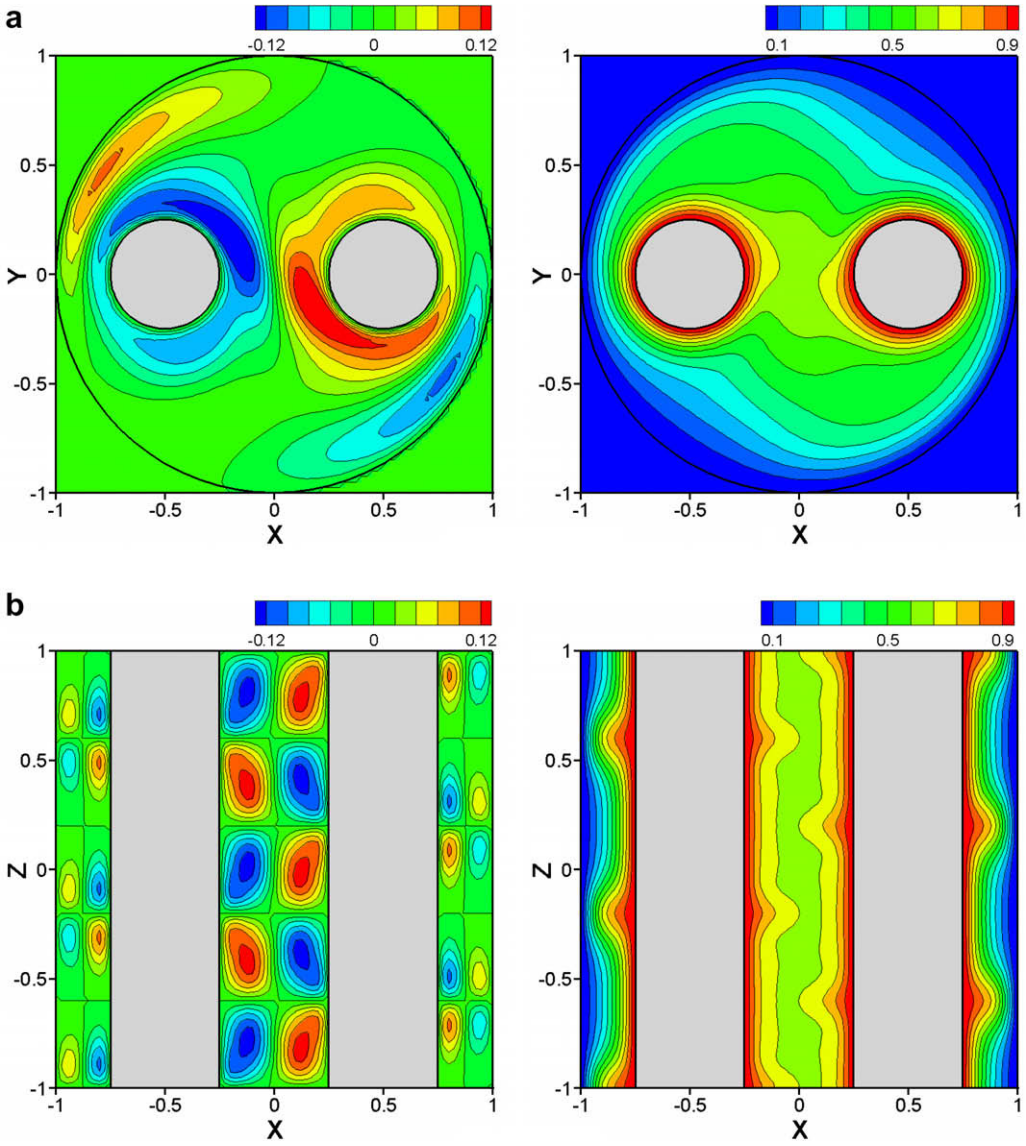

Fig. 3. *w*-contours (left) and isotherms (right) of a co-rotating two-roll mill on (a) $z = 0$ and (b) $y = 0$ planes for Re = 300.

the immersed boundary, and then Gilmanov et al. [12] further followed the lead of Balaras' idea and extended to three-dimensional simulations. We are able to investigate more complex geometry heat and flow problems by just using the simple Cartesian grid. Many fundamental fluid dynamical research problems, such as the 3D two-roll-mill flow, could be further investigated with more details only using this simple Cartesian grid instead of involving complicated mesh generation.

The problem of two-roll-mill flow in the Newtonian fluid is a cylinder that contains two separated inner circular cylinders,

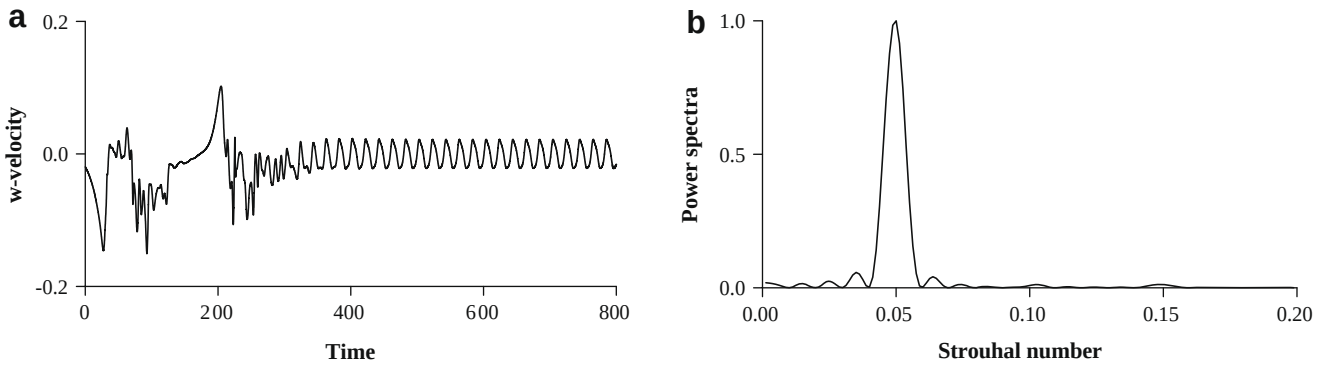

Fig. 4. (a) Time history of *w*-velocity and (b) corresponding spectral analysis of a co-rotating two-roll mill at (0,0,0.2) for Re = 400.

and the flow is generated by the two inner cylinders independently rotating in the fixed locations. Similar to the previous mentioned Taylor–Couette flows, the devices of the two-roll-mill system have potential to produce hydrodynamic instability and vertical vortical motion. Few studies are attempted to solve the 3D Navier–Stokes equations of the two-roll-mill flow due to huge computational cost and numerical limitation. Usually the numerical simulations are implemented under the idealization of an infinitely long cylinder by ignoring the end wall effects. The 2D assumption of the two-roll-mill system is an

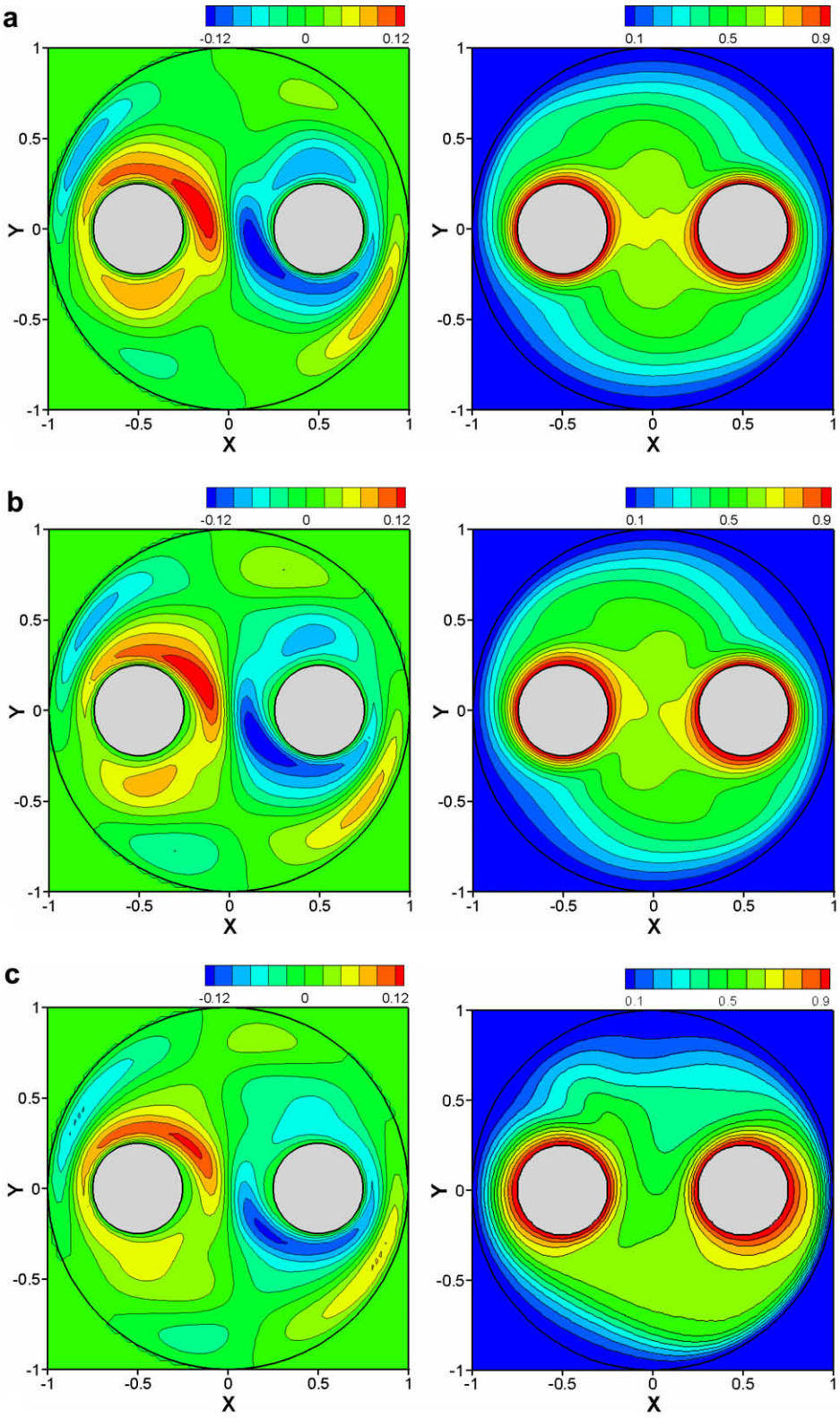

Fig. 5. *w*-contours (left) and isotherms (right) of a co-rotating two-roll mill on $z = 0$ plane at: (a) $t = 610$; (b) $t = 615$; (c) $t = 620$ for Re = 400.

approximation to greatly simplify the simulation efforts. In the authors' previous study [13], the cross sectional heat and flow patterns of a two-roll-mill flow are predicted by using the 2D hybrid Cartesian/immersed-boundary finite-element method. We have attempted to confine our attention to a range of moderate Reynolds numbers for these 2D heat and flow simulations. However, the validity of the existence of axisymmetric flows for meeting the requirement of 2D flow assumption needs further examination when the Reynolds number is increased, and it motivates us to revisit the problem with a fully 3D model.

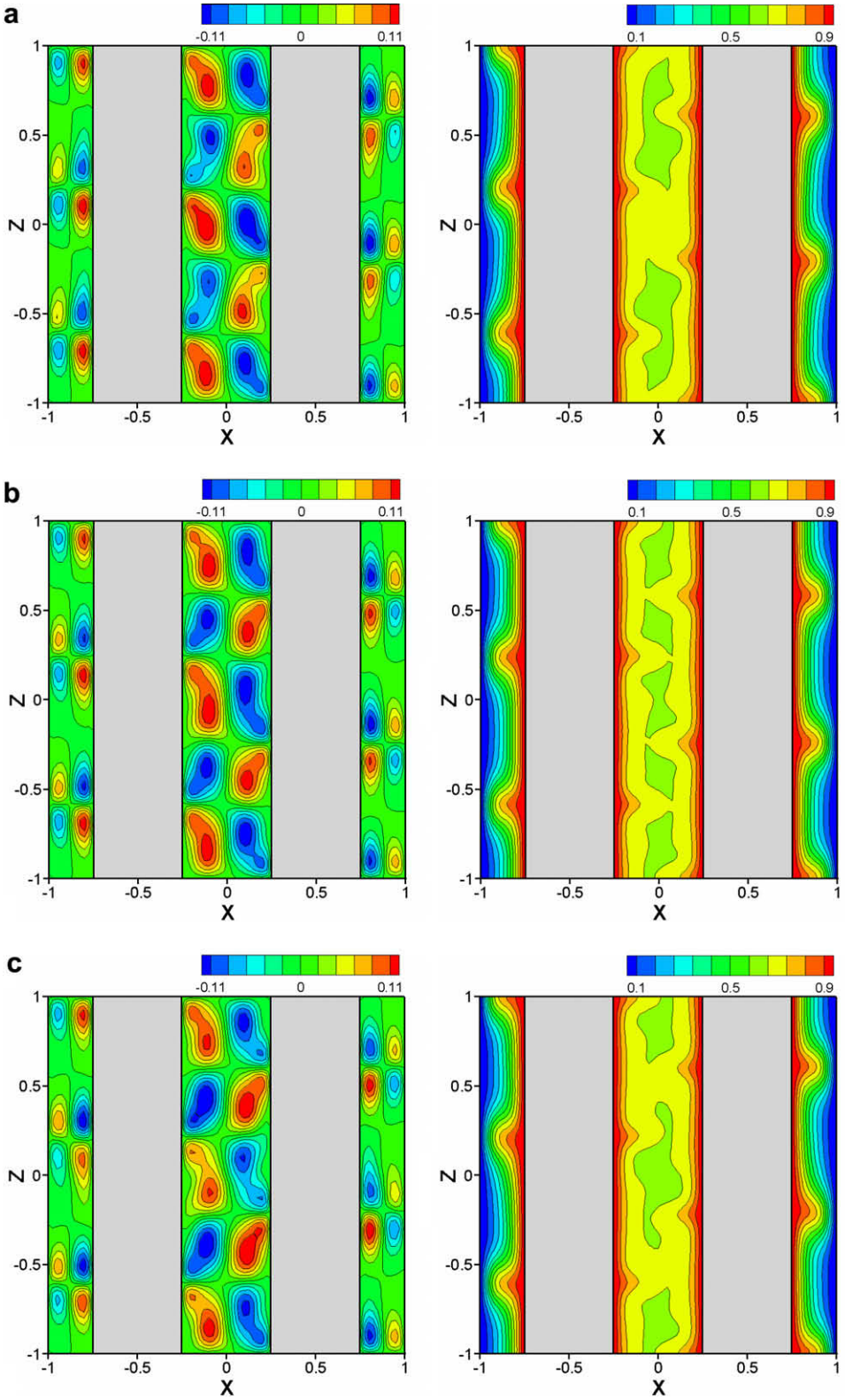

Fig. 6. *w*-contours (left) and isotherms (right) of a co-rotating two-roll mill on $y = 0$ plane at: (a) $t = 610$; (b) $t = 615$; (c) $t = 620$ for Re = 400.

The heat transfer of such complex rotating system is also of great concern in this study, so the two cylinders and the surface of the cavity are imposed with constant but different temperatures. The aim of this article is to establish a fully time-dependent three-dimensional Navier–Stokes model to investigate the realistic 3D heat and flow behaviors of the two-roll-mill system. It is expectable that three-dimensional solutions of the Navier–Stokes equations in flow regimes will be quite different from two dimensions such as the vortex stretching phenomenon. Special attention is paid to study the vertical vortex structure and the hydrodynamic instability in this 3D model. Meanwhile we will make a detailed comparison

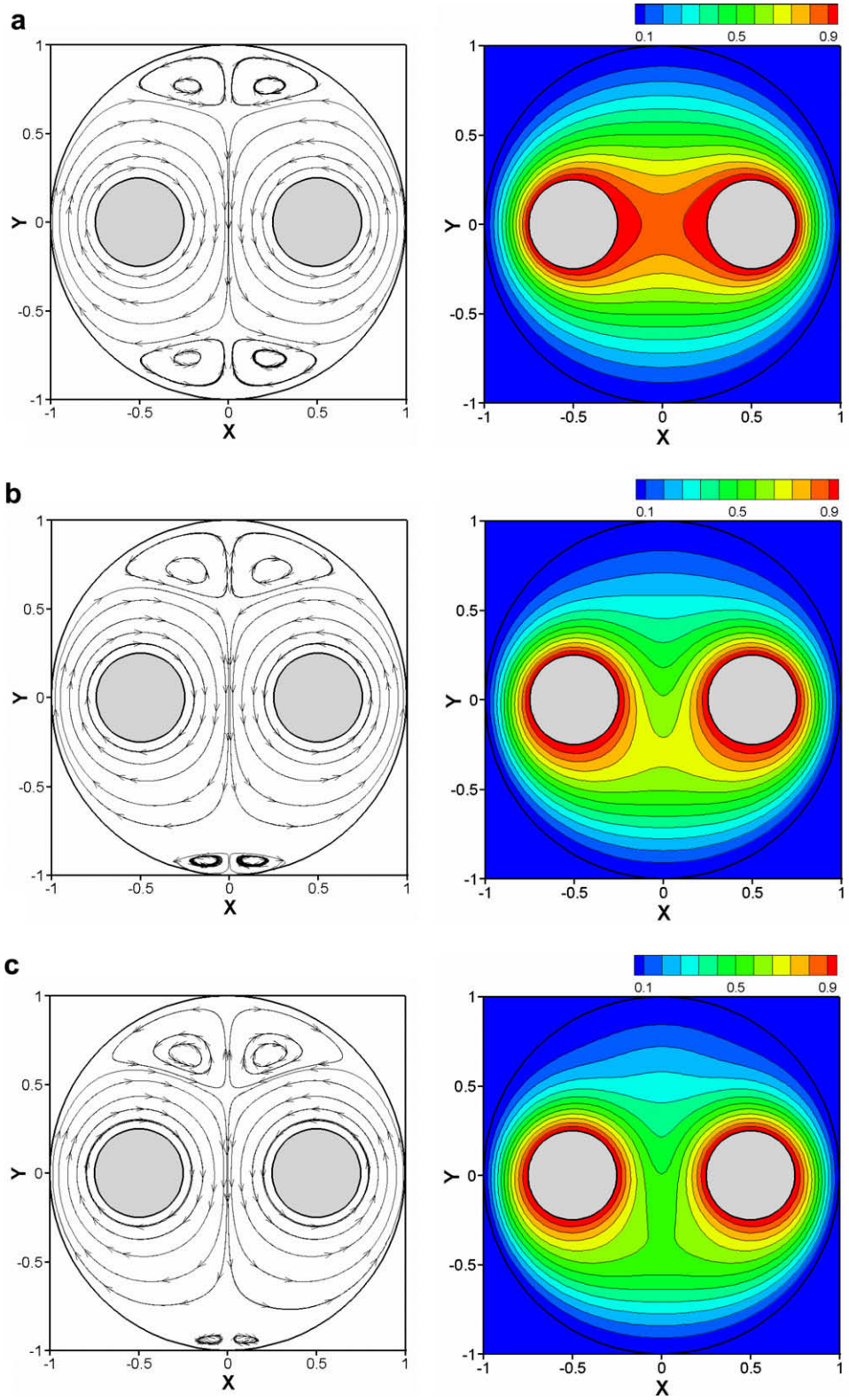

Fig. 7. Streamlines (left) and isotherms (right) of a counter-rotating two-roll mill on $z = 0$ plane for: (a) Re = 0.1; (b) Re = 100; (c) Re = 200.

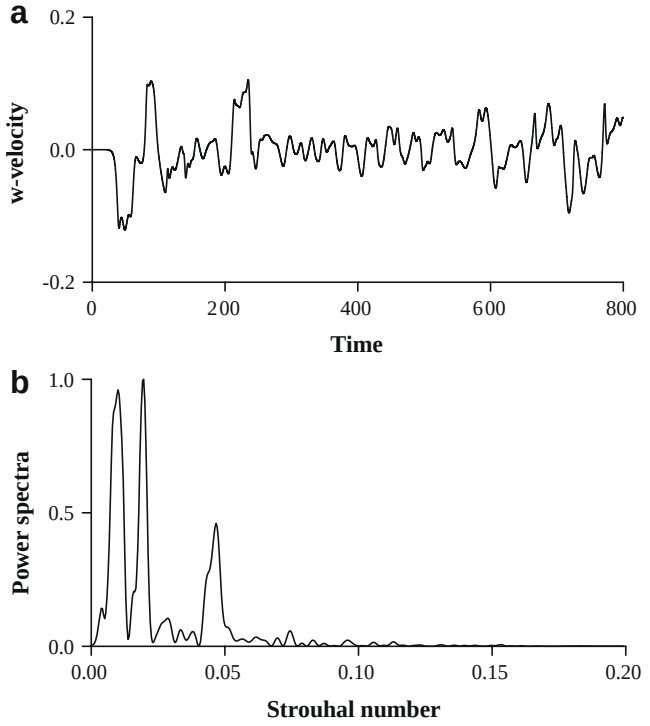

Fig. 8. (a) Time history of *w*-velocity and (b) corresponding spectral analysis of a counter-rotating two-roll mill at (0,0,0.2) for Re = 300.

between the numerical results of previous 2D and present 3D flow and heat simulations to further understand the salient physics of the two-roll-mill problem.

2. Numerical model

2.1. Description of the governing equations and operator-splitting scheme

The incompressible Navier–Stokes equations and the energy equation for forced convection are expressed in primitive-variable form as Eqs. (1)–(3).

$$\nabla \cdot \mathbf{u} = 0 \tag{1}$$

$$\frac{\partial \mathbf{u}}{\partial t} + (\mathbf{u} \cdot \nabla)\mathbf{u} = -\nabla p + \frac{1}{\mathrm{Re}}\nabla^2 \mathbf{u} \tag{2}$$

$$\frac{\partial T}{\partial t} + (\mathbf{u} \cdot \nabla)T = \frac{1}{\mathrm{RePr}}\nabla^2 T \tag{3}$$

in which $\mathbf{u} = (u, v, w)$, T and p are the dimensionless velocity vector, temperature and pressure, respectively. The notations of Re and Pr represent the Reynolds number and Prandtl number. For details of non-dimensionalized process and characteristic parameters, Young et al. [13] is referred.

An operator-splitting scheme with the balanced tensor diffusivity (BTD) [14] term is used to advance the solutions of the 3D Navier–Stokes equations in temporal discretization. The operator-splitting scheme calculates the intermediate or provisional velocities by dropping the pressure term from the momentum equations. Then the intermediate velocities are corrected by using the pressure term to satisfy the incompressibility constraint from the continuity equation. For a fast calculation, we will use an explicit time advancement scheme to solve the advection–diffusion equation, and then compensate the explicit discretization of the convective transport by the BTD term. In this study, the operator-splitting procedure is summarized in the following four steps.

Step 1. Intermediate velocity

$$\frac{\mathbf{u}^* - \mathbf{u}^n}{\Delta t} = -(\mathbf{u}^n \cdot \nabla)\mathbf{u}^n + \frac{1}{\mathrm{Re}}\nabla^2 \mathbf{u}^n + \frac{\Delta t}{2}(\mathbf{u}^n \cdot \nabla)[(\mathbf{u}^n \cdot \nabla)\mathbf{u}^n] + \mathbf{f} \tag{4}$$

Step 2. Pressure calculation

$$\nabla^2 p^{n+1} = \frac{1}{\Delta t}\nabla \cdot \mathbf{u}^* \tag{5}$$

Step 3. Velocity correction

$$\mathbf{u}^{n+1} = \mathbf{u}^* - \Delta t(\nabla p^{n+1}) \tag{6}$$

Step 4. Temperature calculation

$$\frac{T^{n+1} - T^n}{\Delta t} = -(\mathbf{u}^n \cdot \nabla)T^n + \frac{1}{\mathrm{RePr}}\nabla^2 T^n + \frac{\Delta t}{2}(\mathbf{u}^n \cdot \nabla)[(\mathbf{u}^n \cdot \nabla)T^n] + \mathrm{h} \tag{7}$$

In which $\mathbf{u}^*$ represents the intermediate velocity vector, $\mathbf{f}$ and h are the forcing terms used to make the $\mathbf{u}$ and T at $n + 1$ time level satisfy the desired boundary conditions.

2.2. Evaluation of the forcing functions

To satisfy the boundary conditions, the direct forcing concept as proposed by Mohd-Yusof [9] is added to the governing equations near or inside the immersed boundary. The direct forcing is a discrete-time forcing which is obtained in the context of the discretized equation. For example, by considering an advection–diffusion equation, Eq. (7), we can calculate the direct forcing, h, by replacing the T^{n+1} with the desired boundary temperature T_b and rearranging the equation as follows.

$$h = \frac{T_\mathrm{b} - T^n}{\Delta t} + (\mathbf{u}^n \cdot \nabla)T^n - \frac{1}{\mathrm{RePr}}\nabla^2 T^n - \frac{\Delta t}{2}(\mathbf{u}^n \cdot \nabla)[(\mathbf{u}^n \cdot \nabla)T^n] \tag{8}$$

Obviously, the desired temperature is available after adding the forcing into the advection–diffusion equation. Similarly, the direct forcing function for the desired boundary velocity $\mathbf{u}_\mathrm{b}$ takes the following equation.

$$\mathbf{f} = \frac{\mathbf{u}_\mathrm{b} - \mathbf{u}^n}{\Delta t} + (\mathbf{u}^n \cdot \nabla)\mathbf{u}^n - \frac{1}{\mathrm{Re}}\nabla^2 \mathbf{u}^n + \nabla p^n - \frac{\Delta t}{2}(\mathbf{u}^n \cdot \nabla)[(\mathbf{u}^n \cdot \nabla)\mathbf{u}^n] \tag{9}$$

The direct forcing is only imposed on the points located near and inside the immersed boundary; in contrast, both the $\mathbf{f}$ and h terms are set to zero to make the Eqs. (4) and (7) correspond to the basic operator-splitting scheme for the fluid points outside the immersed boundary.

2.3. Interpolation for the desired boundary conditions

The direct forcing is introduced to make the specific grid points to satisfy the given boundary values. However, one important issue inherent in the use of the immersed boundary techniques is that the immersed boundary usually does not coincide with the Cartesian grid. To represent the complex geometry on the Cartesian grid, the original boundary conditions over the immersed

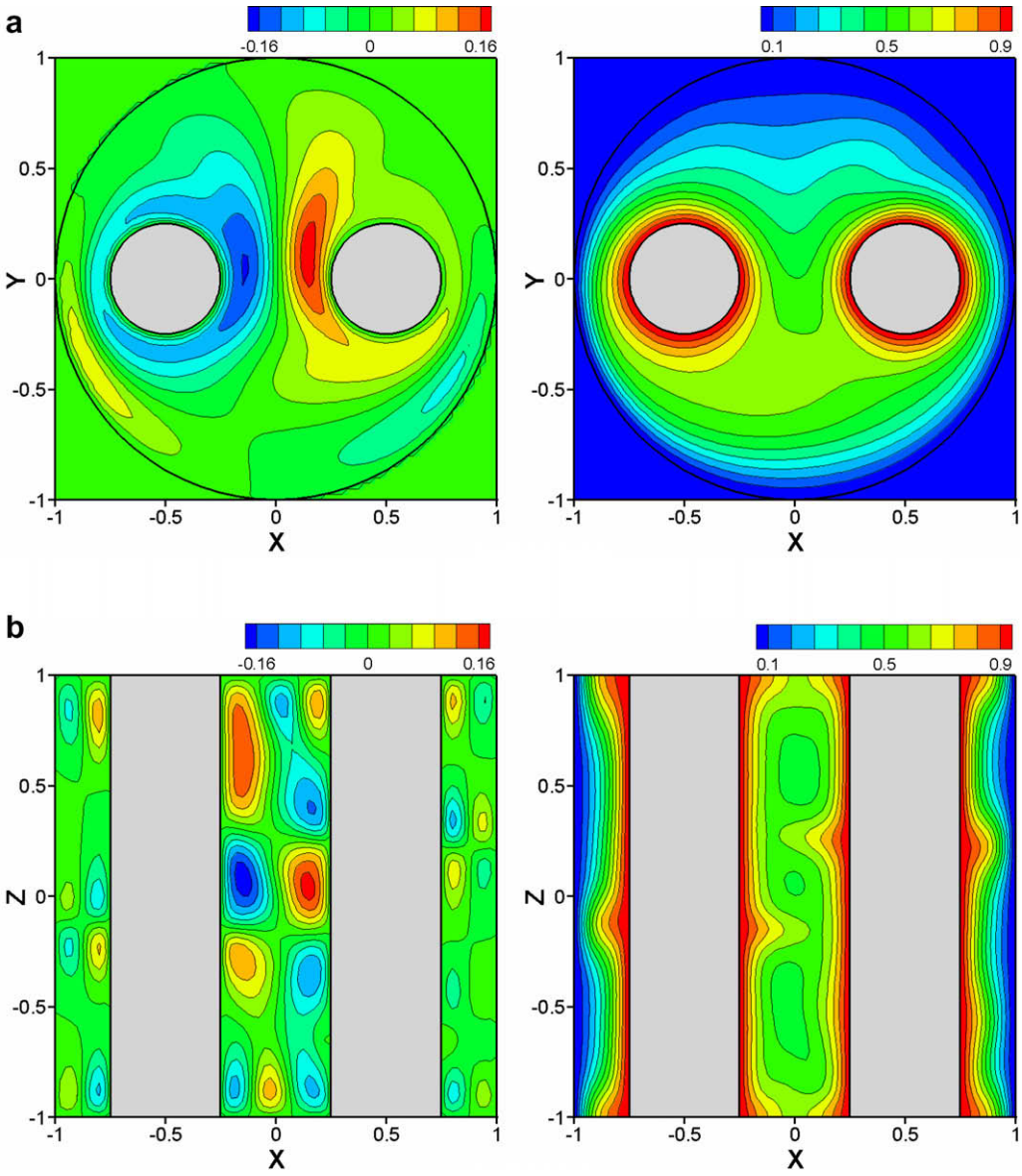

Fig. 9. *w*-contours (left) and isotherms (right) of a counter-rotating two-roll mill on (a) $z = 0$ and (b) $y = 0$ planes at $t = 300$ for Re = 300.

boundary are transmitted via the interpolation procedure to the desired values on the Cartesian grid points. The basic concept is to reconstruct the first point external to the immersed boundary with the desired boundary velocity and temperature, where the corresponding desired boundary values are evaluated using interpolation along the local normal to the solid boundary. The similar interpolation technique is also reported by Refs. [11–13]. However, it is noted that this interpolation technique requires the grids to be fine enough in the neighbor region of immersed boundary to meet linear-approximation assumption of velocity and temperature profiles with proximity to the embedded body. For further detailed description of the interpolation technique, we refer to Young et al. [13].

3. Two-roll mill with independently rotating cylinders

We consider a stationary circular cylinder containing two independently rotating circular cylinders; the cylinder is filled with a Newtonian fluid of Prandtl number 0.71. In the previous study [13], we make the usual simplifying assumptions of two dimensions that the two-roll mill has infinite length in the vertical or axial direction. The end wall effects are totally ignored, and the flow is without vertical perturbation. With these restrictive assumptions, the 2D Navier–Stokes model could be used to simulate the heat and flow patterns in the cross section of the two-roll mill. In contrast, present study of the two-roll mill is of finite height H and the periodic condition is imposed on the top and end walls. The problem of interest is sketched in Fig. 1 including the geometric configuration and the computational-grid system. The outer circular cylinder with a radius $R = 1$ centered on the origin, and the two inner cylinders with radius $r = 0.25$ have centers lying on the horizontal axis of symmetry with a separation of R. The height of two-roll mill is equal to the diameter of the outer circular cavity as $H = 2$. The computational domain is $2R \times 2R \times 2R$ in the x, y and z directions, and a uniform $81 \times 81 \times 81$ grid is used. No-slip boundary conditions are specified on the fluid–solid interfaces; meanwhile constant but different temperatures are imposed on the mill surfaces and two inner cylinders. The temperature is

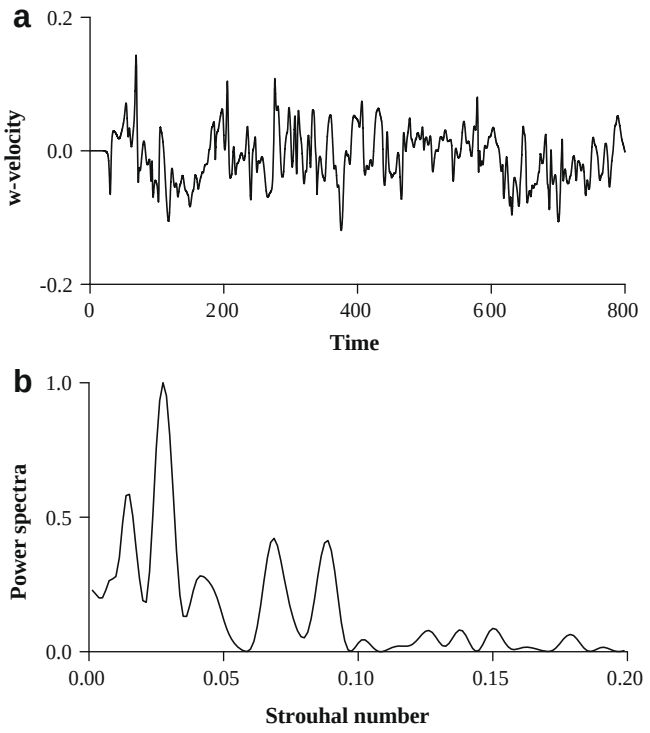

Fig. 10. (a) Time history of *w*-velocity and (b) corresponding spectra analysis of a counter-rotating two-roll mill at (0,0,0.2) for Re = 400.

non-dimensionalized by the difference between surface temperature of the outer and inner cylinders. The two parameters, ϕ_1 and ϕ_2, are defined for the angular velocities of the left and right inner cylinders, respectively. In this system, the Reynolds number is defined by the tangent velocity of the rotating cylinder and the radius of the outer cylinder.

The main concern in this study is the three-dimensional heat and flow patterns in a two-roll mill system induced by different rotating speeds of the inner cylinders. We investigate two case studies which correspond to: (1) co-rotating cylinders; and (2) counter-rotating cylinders. The simulations are performed at increasing Reynolds number, Re = {0.1, 100, 200, 300, 400}, so that the characteristics of different flow regimes can be studied.

3.1. Co-rotating cylinders

In the co-rotating case, the cylinders co-rotate with the same angular speed ($\phi_1 = \phi_2 = 4$).

(a) *Re = 0.1:* For the Stokes flow regime, the flow motions are confined in the azimuthal and radial directions due to the axisymmetric dynamics and the lack of convective effect. Since the flow field is invariant along the axial direction for such a low Re, Fig. 2(a) shows the streamlines and isotherms on $z = 0$ plane to represent the heat and flow patterns for any cross section of the 3D two-roll mill. At Re = 0.1, we have streamline symmetry in $x = 0$ with v-velocity equal to zero, so the streamline is normal to the symmetric line. There exists a saddle point lying midway between the two inner cylinders. Due to the neglect of the fluid inertia, the streamline and temperature plots in Fig. 2(a) exhibit the symmetric characteristics of flow variables as expected for the Stokes flow.

(b) *Re = 100 and 200:* The numerical simulations report that the axial perturbation is still suppressed as the Reynolds number up to 200. Fig. 2(b) and (c) represents the heat and flow patterns of the cross section on $z = 0$ plane at Re = 100 and 200 which can be compared with Fig. 2(a) to show the influence of inertial effect. A saddle point lying midway between the two inner cylinders is preserved with the increasing Reynolds number. The symmetries associated with the Stokes flow are broken as the inertial effects start to play a vital role. The streamlines near the cylinders are approximately the same for the different Reynolds numbers, but a remarkable change of the shape of streamlines is observed in the recirculation regions. When Reynolds number keeps increasing, the vortices will grow larger and larger, and the heat and flow patterns are skewed in the counterclockwise direction.

(c) *Re = 300:* Further increase of the Reynolds number makes the flow become unstable due to the axial perturbations. As the time evolves, vertical motions are initialized and the resulting 3D flow consists of an axial velocity. Fig. 3 depicts the contours of *w*-velocity and temperature distributions at the horizontal plane of $z = 0$ and the meridian plane of $y = 0$, respectively. The cross section contour illustrates that the maximum axial velocity occurs around the two different cylinders with the opposite direction. There are five pairs of vortex cells between the two co-rotating cylinders on the $y = 0$ plane, and the vortex structure is very similar to the Taylor vortex of the Taylor–Couette flow. The peaks of temperature contour occur at the separation points of two different vortex cells, and also arrange in a staggered manner between the two cylinders.

(d) *Re = 400:* As the Reynolds number increases to 400, the flow becomes unsteady and oscillates in a regular manner after transitional region. Fig. 4 records the periodic behavior of the *w*-velocity and its corresponding spectral analysis at the probe point (0,0,0.2). Figs. 5 and 6 illustrate the sequent *w*-contour and isotherm plots on the $z = 0$ and $y = 0$ planes for the periodic oscillations, respectively. A significance to note is that the peak of temperature distribution also periodically moves along the cylinders.

3.2. Counter-rotating cylinders

In the counter-rotating case, the two inner cylinders are rotating with equal but opposite angular velocities ($\phi_1 = -4$, $\phi_2 = 4$).

(a) *Re = 0.1:* At the Stokes flow regime, the flow field generated by counter-rotating cylinders is also invariant along the axial direction for such a low Re. Fig. 7(a) illustrates the streamline and temperature plots of the counter-rotating two-roll mill on the cross section $z = 0$ plane for the Stokes flow regime. Due to the reflectional symmetry of both the geometry and dynamic system at $x = 0$, a saddle point is essentially replaced by a streamline of separation between the two cylinders. The flow patterns are separated by a vertical portion of streamline, and no fluid can cross from the left to the right side or vice versa. The streamlines of the main flow around each cylinder are very circular-like, which are similar in appearance to a single cylinder configuration. Meanwhile, two pairs of recirculation eddies appear at the top and bottom, and these two couple gyres also show the symmetry with respect to $y = 0$ plane.

(b) *Re = 100 and 200:* As the Reynolds number grows to 200, the flow motion remains confirmed to the 2D flow scenario on the cross section of the two-roll mill system. The numerical results of streamline and isotherm plots for the Reynolds numbers of 100 and 200 on $z = 0$ plane are shown in Fig. 7(b) and (c), respectively. With the increasing Reynolds number, the upper eddies grow in size and start moving toward main flow; in contrast, the lower eddies are compressed by the main flow. It should be emphasized that the flow in these cells is extremely weak (secondary flow) in comparison with the neighborhood of cylinders (primary flow). According to no significant changes appearing in the isothermal distributions, it is concluded that the heat transfer is dominated by the diffusion process in the lower recirculation section.

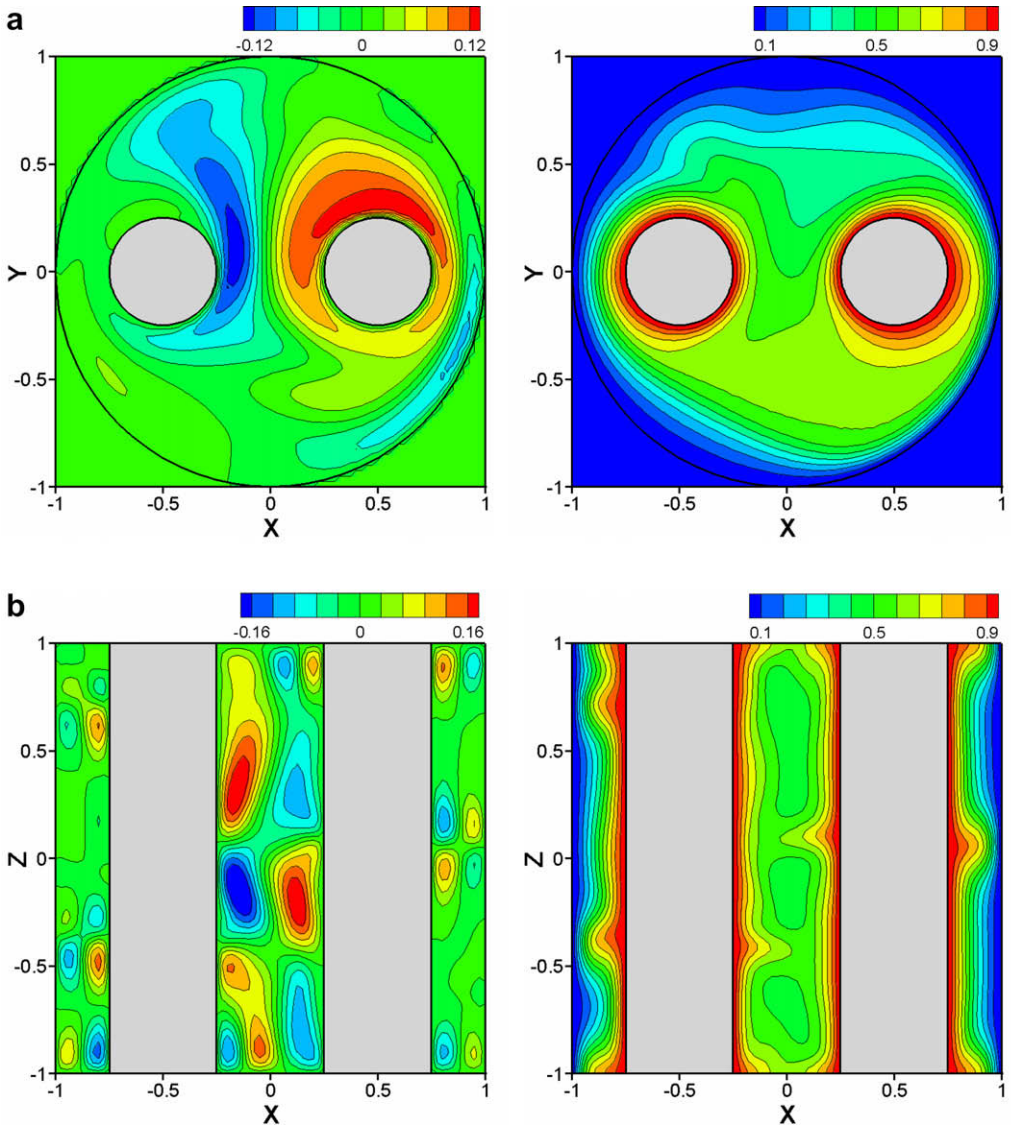

Fig. 11. *w*-contours (left) and isotherms (right) of a counter-rotating two-roll mill on (a) $z = 0$ and (b) $y = 0$ planes at $t = 620$ for Re = 400.

(c) *Re = 300:* At Re = 300, the flow becomes unstable due to axial perturbations, and the hydrodynamic instability is triggered by the growing inertial effect. Fig. 8 records the time history of the *w*-velocity at the probe point (0,0,0.2) and the corresponding spectral analysis after the transitional region. Although the velocity oscillation seems more regular after $t = 300$, the main-frequency is not conspicuous and many sub-frequencies are observed. Fig. 9 displays *w*-contours and isotherms of a counter-rotating two-roll mill system for Re = 300 on $z = 0$ and $y = 0$ planes at $t = 300$. The vortex structure is very complicated which also reflects on the temperature distribution.

(d) *Re = 400:* As the Reynolds number grows from 300 to 400, the flow system exhibits the hydrodynamic instability and becomes more violent with increasing inertia effect. The evolution of *w*-velocity component from $t = 0$ to $t = 800$ at the probe point (0,0,0.2) and the corresponding spectral analysis are described in Fig. 10. According to the records of velocity oscillation and its spectra, the two-roll-mill flow with counter-rotating cylinder for Re = 400 could be categorized into the chaotic flow. Fig. 11 displays *w*-contours and isotherms of a counter-rotating two-roll mill on the horizontal plane of $z = 0$ and the meridian plane of $y = 0$ for Re = 400 at $t = 620$. The heat patterns are very complicated and strongly varied with time. In the meantime the wave-like isotherms seem to travel up and down along the two cylinders.

3.3. Numerical validations

In the above section, the 3D hybrid Cartesian/immersed-boundary method is used to capture the numerous physical phenomena in a two-roll mill system. The reliability of the developed model is judged by the reasonable physical characteristics. As mentioned previously, the main issue of the immersed-boundary method is that the immersed boundary does not coincide with the Cartesian grid, so that the given boundary conditions on the immersed boundary are transmitted to the desired values over the Cartesian grid with a linear approximation. Once the desired values are obtained, we can reconstruct the velocity and temperature on the first points external to the immersed boundary. Fig. 12 illustrates a close look at the streamline and isotherm near the right cylinder of the co-rotating case at Re = 100. Since the flow is generated by the inner cylinder and the heat transfer is dominated by the diffusion effect in this region, it is expectable that the streamline and the isotherm close to the cylinder should exhibit the shape of the cylinder. Although only 20 grid points in *x* and *y* directions are uniformly

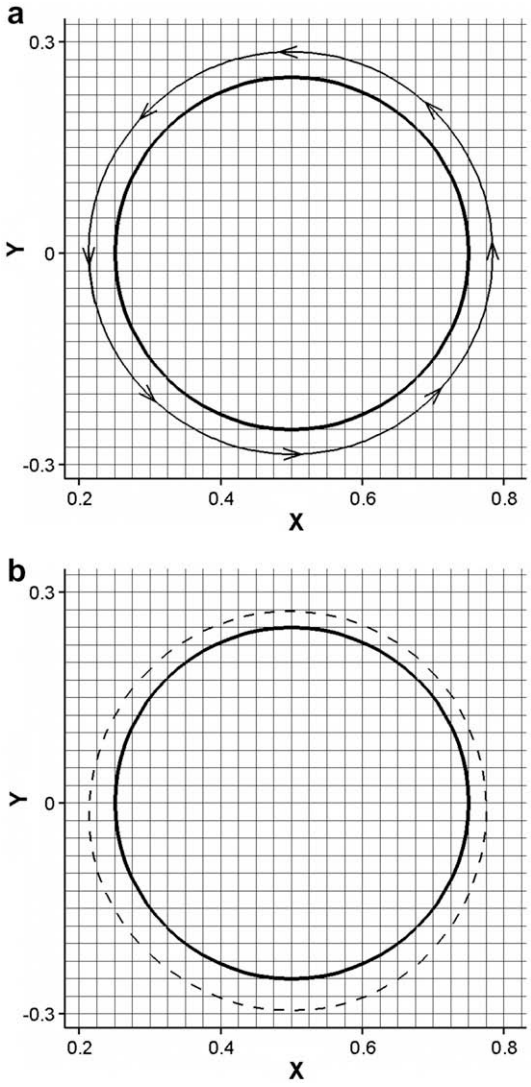

Fig. 12. (a) Streamline and (b) isotherm $T = 0.9$ around the right cylinder on $z = 0$ plane for co-rotating case of Re = 100.

distributed within the inner cylinder diameter, the streamline next to the cylinder forms a well closed loop and the isotherm, $T = 0.9$, is distributed in a very smooth manner without obvious stepwise geometry. The reasonable predictions in the near-wall zone demonstrate the capability of the adopted interpolation scheme for representing the effects of embedded body on the Cartesian grid.

To analyze the accuracy of overall numerical procedure, the simulations of the co-rotating case at Re = 100 are revisited using three different grids ranging from $61 \times 61 \times 81$, $81 \times 81 \times 81$ up to $101 \times 101 \times 81$ uniformly in the x, y and z directions, respectively. The results of grid-independence study are demonstrated in Fig. 13, judging from the fact that different grid levels make no significant change in the computed velocity and temperature profiles along $x = 0$ and $z = 0$. In authors' previous study [13], the 2D hybrid Cartesian/immersed-boundary finite-element model is developed to simulate the two-roll-mill flow with the axisymmetric assumption, and the results are also illustrated in Fig. 13 or co-rotating case of Re = 100. The mesh-independent solutions for the present 3D model are almost indistinguishable in comparison with the previous 2D results. Before the flow becomes unstable due to axial perturbations, the present 3D model has capacity to render the 2D result for the simple flow flied without the provision of axisymmetric assumption.

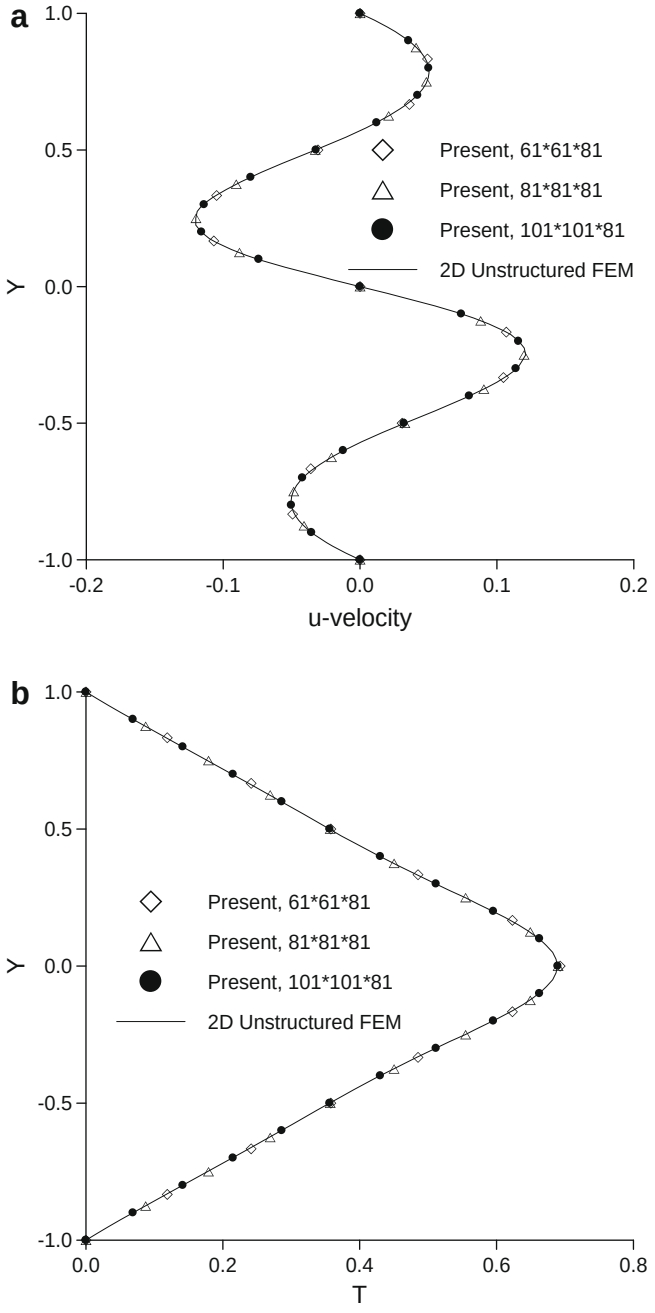

Fig. 13. (a) u-velocity and (b) temperature profiles along $x = 0$ and $z = 0$ with different grid numbers for co-rotating case of Re = 100.

4. Conclusions

The two-roll-mill flow is of fluid dynamic importance and also has many practical applications. A hybrid Cartesian/immersed-boundary finite-element model has been developed to allow us to simulate fully 3D unsteady, viscous incompressible flows and heat transfers within the two-roll-mill system generated by the two inner rotating cylinders. The framework of the developed model contains: (1) the Gelerkin finite-element procedure in which structured prism element is utilized to discrete the computation domain; (2) the operator-splitting scheme with the BTD term is used to advance the solution in time; (3) the hybrid Cartesian/immersed-boundary method is employed to deal with complex geometry over a Cartesian grid. The physical characters,

streamline topologies and temperature contours are discussed for a range of the rotating velocities and Reynolds numbers. The flow regimes are characterized by 3D features of the non-axisymmetry, the vertical vortex structure and the hydrodynamic instability. Based on the numerical results, several conclusions are drawn as follows:

1. For the counter-rotating case, the fluid motion between the cylinders is reinforced in a uniform direction, and results in a stronger velocity in comparison with the co-rotating case which the driven forces are counteracted in this region. As a result, the flow field of the counter-rotating case is therefore more violent and the unstable behavior is expected to occur here for lower rates of rotation. In our numerical experiment, the two-roll-mill flows are confirmed to 2D motion as the Reynolds numbers equal to 0.1, 100 and 200 for both the co- and counter-rotating cases. However, for the co-rotating case, the flow breaks the axisymmetry and is finally replaced by the cellular pattern on the axial plane at Re = 300; as the Reynolds number further increases to 400, the flow will oscillate with a single frequency. As for counter-rotating, the time history of w-velocity and its power spectra show the chaotic flow regime for the Reynolds number larger than 300. This event reveals that the counter-rotating is more powerful for creating chaotic advection than the co-rotating in the two-roll-mill system.
2. The assumption of axisymmetry in the two-roll-mill system is usually regarded as an approximate approach to simplify the numerical simulation and to reduce the computational cost since a 2D model can be made. However, a model with axisymmetric assumption is very restrictive to describe the realistic flow behaviors. The present 3D results of computed velocity and temperature profiles along $x = 0$ and $z = 0$ for Re = 100 are compared well with the previous 2D simulation. The results demonstrate that when the axisymmetric characteristics should be maintained, the 3D numerical result will automatically render the subset of the axisymmetric flow patterns. However, as the Reynolds number exceeds a critical value, the non-axisymmetric nature will prohibit the usage of the axisymmetric assumption and require a 3D model. The developed fully three-dimensional model has demonstrated a considerable capacity to capture the realistic physical phenomena, even for the chaotic flow regime.
3. In view of the heat and mass transfer, the unsteady and oscillating flow phenomenon is a very efficient way to amplify the heat transfer augmentation. Among the unsteady and oscillating flow systems, the chaotic flows have distinct advantages over the non-chaotic flows. Up to the Re = 200, the two-roll-mill flows are steady and confirmed to 2D motion, so the axial transfer is limited by a simple diffusion. For the co-rotating case at Re = 300, the cellular pattern appears and the peaks of temperature contour occur at the separation points of two different vortex cells on the axial plane. The vortex cells are still inefficient mixers, because each vortex remains disconnected from its neighbors. As flows grow into unsteady and oscillating regimes, it is observed that the peaks of isotherm are similar to the traveling wave which propagates along the cylinders up and down. When the flow velocity oscillates in a simple periodic manner, the wave will also propagate with a single frequency. As the flow becomes chaotic motion, the temperature will change rapidly with time, such that the fluid mixing is enhanced considerably.

Acknowledgment

The National Science Council of Taiwan is greatly appreciated for providing financial support of this research under the Grant No. NSC 96-2811-E-002-040.

References

[1] V. Sobolik, B. Izrar, F. Lusseyran, S. Skali, Interaction between the Ekman layer and the Couette–Taylor instability, Int. J. Heat Mass Transfer 43 (24) (2000) 4381–4393.
[2] T.M. Jeng, S.C. Tzeng, C.H. Lin, Heat transfer enhancement of Taylor–Couette–Poiseuille flow in an annulus by mounting longitudinal ribs on the rotating inner cylinder, Int. J. Heat Mass Transfer 50 (1–2) (2007) 381–390.
[3] M. Rudman, Mixing and particle dispersion in the wavy vortex regime of Taylor–Couette flow, AIChE J. 44 (5) (1998) 1015–1026.
[4] C.B. Liao, S.J. Jane, D.L. Young, Numerical simulation of three-dimensional Couette–Taylor flows, Int. J. Numer. Methods Fluids 29 (7) (1999) 827–847.
[5] H.A. Stone, Dynamics of drop deformation and breakup in viscous fluids, Annu. Rev. Fluid Mech. 26 (1994) 65–102.
[6] M.A.H. Reyes, E. Geffroy, A corotating two-roll mill for studies of two-dimensional elongational flows with vorticity, Phys. Fluids 12 (10) (2000) 2372–2376.
[7] T.J. Price, T. Mullin, J.J. Kobine, Numerical and experimental characterization of a family of two-roll-mill flows, Proc. R. Soc. A 459 (2029) (2003) 117–135.
[8] C.P. Hills, Flow patterns in a two-roll mill, Q. J. Mech. Appl. Math. 55 (2) (2002) 273–296.
[9] J. Mohd-Yusof, Combined Immersed-boundary/B-Splines Methods for Simulations of Flow in Complex Geometries, CTR Annual Research Briefs, Center for Turbulence Research, NASA Ames/Stanford University, 1997.
[10] E.A. Fadlun, R. Verzicco, P. Orlandi, J. Mohd-Yusof, Combined immersed-boundary finite-difference methods for three-dimensional complex flow simulations, J. Comput. Phys. 161 (1) (2000) 35–60.
[11] E. Balaras, Modeling the complex boundaries using an external force field on the fixed Cartesian grids in large-eddy simulations, Comput. Fluids 33 (3) (2004) 375–404.
[12] A. Gilmanov, F. Sotiropoulos, E. Balaras, A general reconstruction algorithm for simulating flows with complex 3D immersed boundaries on Cartesian grids, J. Comput. Phys. 191 (2) (2003) 660–669.
[13] D.L. Young, C.L. Chiu, C.M. Fan, A hybrid Cartesian/immersed-boundary finite-element method for simulating heat and flow patterns in a two-roll mill, Numer. Heat Transfer B 51 (3) (2007) 251–274.
[14] P.M. Gresho, S.T. Chan, R.L. Lee, C.D. Upson, A modified finite element method for solving the time-dependent incompressible Navier–Stokes equations. Part I: Theory, Int. J. Numer. Methods Fluids 4 (6) (1984) 557–598.